RESEARCH ARTICLE

Analysis of Reactive Power Strategies in HVDC–Connected Wind Power Plant Clusters

Kevin Schönleber[1], Sergi Ratés-Palau[1] and Oriol Gomis-Bellmunt[2]

[1]GE Renewable Energy, Roc Boronat 78, 08005 Barcelona, Spain. [2]Centre d'Innovació Tecnològica en Convertidors Estàtics i Accionaments (CITCEA-UPC), Departament d'Enginyeria Elèctrica, Universitat Politècnica de Catalunya, ETS d'Enginyeria Industrial de Barcelona, 08028 Barcelona, Spain.

ABSTRACT

Offshore wind power plants (WPPs) built in the vicinity of each other but far from shore usually connect to the main grid by a common high–voltage DC (HVDC) transmission system. In the resulting decoupled offshore grid, the wind turbine converters and the high–voltage DC voltage–source converter (VSC–HVDC) share the ability to inject or absorb reactive power. The overall reactive power control dispatch influences the power flows in the grid and hence the associated power losses. This paper evaluates the respective power losses in HVDC–connected WPP clusters when applying five different reactive power control strategies. The case study is made for a 1.2–GW–rated cluster comprising three WPPs and is implemented in a combined load flow and converter loss model. A large set of feasible operating points for the system is analyzed for each strategy. The results show that a selection of simulations with equal wind speeds is sufficient for the annual energy production comparison. It is found that the continuous operation of the WPPs with unity power factor has a superior performance with low communication requirements compared to the other conventional strategies. The optimization–based strategy which is developed in this article allows a further reduction of losses mainly due to the higher offshore grid voltage level imposed by the VSC–HVDC. Reactive power control in HVDC–connected WPP clusters change significantly the overall power losses of the system which depend rather on the total sum of the injected active power than on the variance of wind speeds inside the cluster.

KEYWORDS

DOI: 10.1002/we

Prepared using weauth.cls

Wind Energ. 2016; **00**:2–23
Load flow; power system management; reactive power; voltage control; grid integration; wind power plants; hvdc transmission
DOI: 10.1002/we

Correspondence

Kevin Schönleber, GE Renewable Energy, Roc Boronat 78, 08005, Barcelona, Spain. E-mail: kevin.schonleber@ge.com

Contract/grant sponsor

People Programme (Marie Curie Actions) of the European Unions Seventh Framework Programme (FP7/2007-2013).

Contract/grant number

317221

Received . . .

1. INTRODUCTION

Vicinity of very remote offshore wind power plants (WPPs) motivates the use of a common high–voltage DC (HVDC) grid connection to link the power plants to the main grid [1, 2]. Such a scheme is referred as HVDC–connected WPP cluster. Especially in the German North Sea several of these WPP clusters have already been commissioned and operated, namely the converter stations bundled inside the BorWin, DolWin, HelWin, and SylWin clusters [3]. Up to now, radial point–to–point HVDC connections are the preferred solution for coordinated installation of remote offshore wind generation. In the future, it is very likely that an increased penetration of renewable power sources far offshore will shift from those point–to–point connections to an interconnected offshore grid on AC–side as well as meshed configurations on DC–side [4, 5, 6].

The combined power rating of the WPPs is decided in accordance to the HVDC system to avoid stranded investment mutually. At the moment the power rating of high–voltage DC voltage–source converter (VSC–HVDC) systems to connect WPP clusters of 400 to 900 MW is already industrialized [3]. The near–future VSC–HVDC power rating for offshore connection might increase further due to technical innovation e.g. higher DC voltages (± 525 kV). The nature of WPPs to cover areas of several tenth of square kilometers results in extensive medium–voltage (MV) collection grids and inherently in a certain distance between the high–voltage AC offshore substation (HVAC–OS) and the offshore VSC–HVDC substation. Collection grids might be built as radial or meshed grids [2, 7] and the distance between WPP and offshore VSC–HVDC is up to 40 km for today's projects [3, 4]. The offshore grids are characterized by highly variable, unsymmetrical power flows, extensive submarine cabling, and exclusively power converter–based generation.

The ownership boundaries in the offshore grids differ from country to country. In the German North Sea, for instance, the offshore grid is unbundled between the WPP operators and the transmission grid operator interfacing the WPP–side end of the high–voltage AC (HVAC) export cables [8]. The ownership boundaries inherently result in control limitations which are to be considered for overall operation strategies of an HVDC–connected WPP cluster.

In an HVDC–connected WPP cluster the offshore grid operates electrically asynchronous or decoupled from the onshore grid. Usually, the offshore VSC–HVDC regulates voltage and frequency in the offshore grid and sinks all active and reactive power generated. The active power is mainly generated by the wind turbines (WTs), whereas the reactive power is injected or absorbed by the WT transformers, filters, converters, collection grid cables, WPP transformers, shunt compensation devices, HVAC export cables, HVDC transformer, and the VSC–HVDC itself. The group of controllable reactive power devices in the system is limited to the converters, switchable shunt compensations, and on–load tap changer (OLTC) of transformers which either regulate reactive power directly or indirectly through voltage control. WT converters usually provide reactive power during power system faults or as ancillary service [9, 10]. A combined control of these devices represents an optimization problem with the main objective of secure operation and furthermore power loss reduction through enhanced operation. In power systems this principle is usually deployed at transmission grid level [11, 12, 13, 14, 15] as well as proposed for the internal collection grid of AC-connected WPPs [16, 17, 18, 19, 20, 21, 22, 23, 24, 25]. The application of such techniques in HVDC–connected WPPs has been studied in [26, 27]. It was concluded that the best reactive power strategy shares the total amount of reactive power among the WTs on the one side and the VSC–HVDC on the other side. The references [23, 26, 27] suggest the incorporation of converter losses in the loss function to improve the quality of the optimization algorithm. The application of reactive power management in HVDC–connected WPP clusters is of special interest as multiple system and control layers evolve. To the knowledge of the authors, the sole literature published on reactive power management for the WPP cluster application can be found in the technical brochures of the CIGRE working groups B4-55 and B3-36 [3, 28]. Both references identify a potential cost reduction and propose further investigation on this topic.

This paper assesses five reactive power control strategies, both conventional and optimization–based ones, for HVDC–connected WPP clusters. A dedicated model combines power losses in the passive components as well as in the power converters. A benchmark strategy represents the best case scenario for the system to evaluate the performance of the strategies. Furthermore, one optimization–based reactive power control strategy is proposed which is especially suitable for the application in HVDC–connected WPP clusters. Contrary to conventional optimal power flow (OPF) approaches used in power system applications, the proposed strategy considers the power losses caused inside the WPPs due to a

DOI: 10.1002/we

reactive power set–point and utilizes the voltage control capability of the offshore VSC–HVDC. The active power variation is evaluated for several degrees of wind speed variance inside the WPP cluster. The key performance indicator is the annual energy production (AEP) resulting under the operation of the WPP cluster with the respective strategy.

The key findings are anticipated in the following. The exploration of the voltage control capability of the VSC–HVDC with reactive power control in the WPP cluster results in a higher AEP of the system. It is further found that in this application active power variation between the different WPPs (e.g. due to inter–cluster wake effects) barely impact the assessment on reactive power control strategies. Additionally, it is highlighted that unity power factor (PF) operation of the WPPs performs the best among the conventional strategies.

The paper is organized as follows: Section 2 describes the proposed control strategies and the methodology developed to assess their performance. In Section 3, a case study is defined for a WPP cluster consisting of three WPPs. The results are shown in Section 4. The article closes in Section 5 with the discussion and recommendation to the operators.

2. METHODOLOGY

This section is developed in five parts: firstly a general description of the system and power losses under consideration is given and secondly the studied reactive power control strategies are presented. The optimization–based concepts are outlined with their respective objective function and constraints. Finally, further considerations about wind speed data and variance in WPP clusters are given along with a brief discussion about the operational implementation of the reactive power control strategies.

2.1. System description and loss assessment

A generic system sketch of an HVDC–connected WPP cluster is depicted in Figure 1: The n wind power plants $\mathrm{WPP1}$, $\mathrm{WPP2}$, ..., $\mathrm{WPP}n$ with a respective rated power of P_{WPP1}, P_{WPP2}, ... , $P_{\mathrm{WPP}n}$ connect to the offshore VSC–HVDC via high–voltage (HV) submarine cables from their respective HVAC–OS. Each WPP comprises multiple WTs which are linked through radial strings as MV collection grid to the HVAC–OS. The AC voltage level might be 33 kV for the MV collection grid and 155 kV for the HV offshore grid, in line with current projects connected to the Tennet transmission grid [8]. To compensate the capacitive reactive current in the HV offshore grid due to the shunt capacitance of the submarine cables particularly during grid energization and low power conditions, switchable shunt reactors are deployed at the HV cable ending to the HVAC–OS. Being equipped with mechanical no–load switches, the on/off status of these shunt reactors

DOI: 10.1002/we

does not change during normal operation. In contrast to that the WPP transformers comprise an OLTC to be perform tap changes even under load.

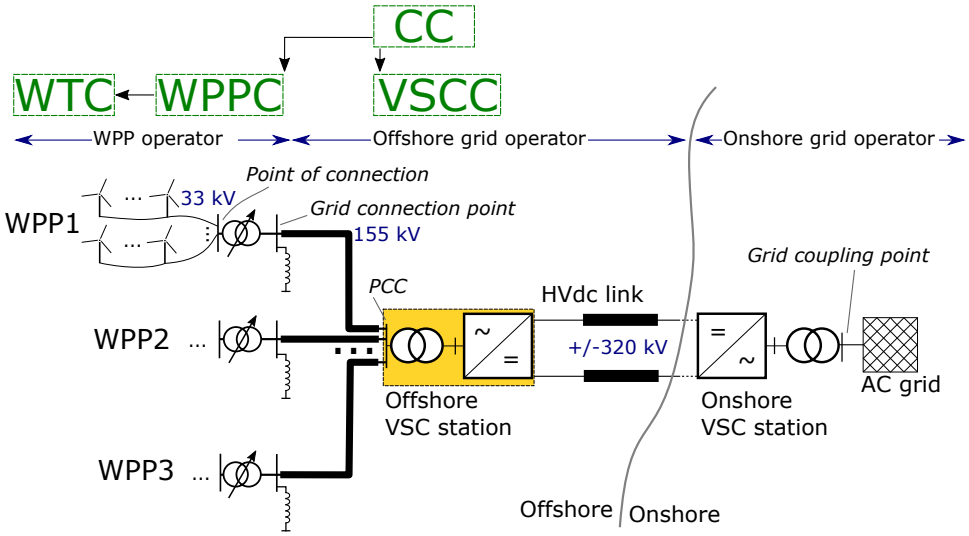

Figure 1. Exemplary HVDC–connected offshore WPP cluster. The labels shown for the busbars in WPP1 are equally respective identifier in the other WPPs.

With reference to the Tennet grid code [8], the admissible voltage range for continuous operation for all components in the offshore grid is $u = 0.9\,\mathrm{p.u.}$ to $1.1\,\mathrm{p.u.}$ (per–unit). The reactive power requirements are defined for the generating units as well as at the grid connection point (HV–side of WPP transformer). As the GC is not limited to HVDC–connected WPPs it describes the possible use of additional compensation devices [e.g. switchable capacitor banks, reactors, or static compensators] to meet the reactive power requirement at the grid connection point. In the presence of a VSC–HVDC, which might also control reactive power, the installation of such additional compensation devices is unusual for normal operation but might be necessary for emergency operation [28]. The minimum requirements for the reactive power capability of the generating units (i.e. WTs) are defined at the low voltage side of the WT transformer. They might be fulfilled by appropriately designed full–scale power converter–based wind turbines (FSC–WTs), usually referred as type 4 turbines, which are capable to provide reactive power even during no wind situations. A FSC–WT has a generator–side converter which is connected via a DC link to a grid–side converter (GSC). The GSC might be designed to be capable providing maximum reactive power exchange with the grid corresponding to a PF of $\cos\varphi = 0.9$ (both inductive and capacitive) at full power. It is assumed that this capability is available over the admissible voltage range for continuous operation.

DOI: 10.1002/we

The overall control hierarchy can be defined according to the schematic shown in Figure 1. First, the internal control of the GSC of each WT, the WT control system (WTC), regulates active and reactive power exchanged with the grid. These set–points (SPs) are subject to limitations depending on the actual operating point of the GSC. The references might be set locally or sent by a superior control system, most commonly the WPP control system (WPPC). The responsibility of the WPPC encloses the control of active and reactive power at the point of connection, which in this paper is the MV–side of the respective WPP transformers. It might incorporate the control of the OLTC and the dispatch of active and reactive power references to the WTs. The VSC–HVDC relies on a proper VSC control system (VSCC) which controls the voltage at the point of common coupling (PCC) bus (the reference voltage might be an external SP). If required by the control concept, a central control (CC) is able to interact with the WPPC and VSCC. The use of the controllers and their communication necessities differ among the reactive power control strategies and is subsequently outlined in Section 2.2.

The reactive power control strategies are evaluated against the overall system losses as the main performance indicator. As stated earlier the offshore grid is decoupled which implies that e.g. commercial use of reactive power is not relevant. The system loss function is defined in (1).

$$P_{\text{system}}^{\text{loss}} = \sum_{i=1}^{n} P_{\text{WPP}i,\text{HV}}^{\text{loss}} + P_{\text{off. grid}}^{\text{loss}} + P_{\text{VSC}}^{\text{loss}} \tag{1}$$

where $P_{\text{WPP}i,\text{HV}}^{\text{loss}}$ represents the power losses inside $\text{WPP}i$ until the HV–side terminal of the WPP transformer, $P_{\text{off. grid}}^{\text{loss}}$ allocates the sum of electrical losses in the HV export cables and $P_{\text{VSC}}^{\text{loss}}$ are the overall VSC–HVDC station losses, respectively.

The assessment might be done with a complete power flow model covering the whole system (VSC–HVDC, offshore grid, WPP collection grids, and WT converters). However, this approach results to be very time–consuming for the analysis of a large number of operating points specifically for the optimization–based approaches and is only used for the benchmark strategy elaborated later. Therefore, the WPP power losses are formulated by means of approximated loss functions. The internal WPP losses $P_{\text{WPP}i,\text{HV}}^{\text{loss}}$ are based on the combined converter loss and power load flow model developed in [26]. When the voltage at the MV–side of the WPP transformer (point of connection) is controlled locally, e.g. to $u_i \approx 1.0\,\text{p.u.}$ by means of the respective OLTC, an approximated WPP loss function $P_{\text{WPP}i,\text{MV}}^{\text{loss}}(p_{\text{WT}}, q_i)$ might be set up in dependence of the active power injection p_{WT} by the WTs and the reactive power injection q_i at the point of connection. Hence, the power losses of a $\text{WPP}i$ at the HV terminals, $P_{\text{WPP}i,\text{HV}}^{\text{loss}}$, as introduced in (1), represents the sum of the power losses inside $\text{WPP}i$ until the MV–side terminal of the WPP transformer, $P_{\text{WPP}i,\text{MV}}^{\text{loss}}$, and the WPP transformer losses. For the

DOI: 10.1002/we

sake of simplicity, the internal reactive power control strategy inside the WPP uses an equal dispatch of reactive power set–points to the WTs, albeit an optimized–based strategy such as described in [26] might be used as well. The approximation function is developed as a mth grade polynomial function with coefficients c_{jk} and is described in (2).

$$P^{\text{loss}}_{\text{WPP}i,\text{MV}}(p_{\text{WT}}, q_i) = \sum_{j=0}^{m}\sum_{k=0}^{m} c_{jk} \cdot p_{\text{WT}}^{j} \cdot q_i^{k} \tag{2}$$

The losses in the offshore grid $P^{\text{loss}}_{\text{off. grid}}$ (and in the WPP transformers $P^{\text{loss}}_{\text{WPP}i,\text{trf}}$ if explicitly specified) are result of load flow calculations using Matpower [29]. The VSC–HVDC station losses $P^{\text{loss}}_{\text{VSC}}$ can be approximated by a constant, linear, and quadratic part in dependence of the converter current as shown in (3) [30, 31].

$$P^{\text{loss}}_{\text{VSC}} = \left[a + b \cdot \frac{I_c}{I_r} + c \cdot \left(\frac{I_c}{I_r}\right)^2\right] \cdot S_r \tag{3}$$

where a, b, and c are converter–specific loss coefficients, I_c and I_r are the actual and rated converter current, respectively, and S_r is the voltage–source converter (VSC) power rating. Such a loss function might be used for either two– or three–level converters but as well for modular multilevel converter (MMC). The latter is the current state of the art for connection of offshore wind and therefore used in this study. The coefficients differ from those of two–level converter as a MMC has generally lower losses due to the reduced switching frequency [26].

The system loss function $P^{\text{loss}}_{\text{system}}$ is integrated in Matlab using Matpower [29] and fmincon to assess different reactive power control strategies and multiple steady–state operating points.

2.2. Reactive power control strategies

A benchmark strategy is formulated as the optimum steady–state operating point of the system. It is based on an optimization aiming to minimize the system losses under a number of constraints and with the control variables being the reference voltage imposed by the offshore VSC–HVDC and the reactive power injections by the WTs. The restrictions on real–time data access due to communication constraints and/or operator boundaries might disqualify the benchmark strategy in a real implementation. Thus, the sole purpose of this strategy is the evaluation of the others.

- S0: Overall optimization of active power losses by individual WT reactive power set–points q_{WT} and reference voltage u_{PCC} to the VSC–HVDC.

Furthermore, five reactive power strategies for the application in an HVDC–connected WPP cluster are under evaluation:

- S1: WTs are operating at unity power factor ($\cos\varphi = 1$).

DOI: 10.1002/we

- S2: WPPs are operated at unity power factor ($\cos\varphi = 1$).
- S3a: VSC–HVDC is operated at $\cos\varphi = 1$ and offshore grid operator (OGO) dispatches equal q_i set–points to the WPPs.
- S3b: VSC–HVDC is operated at $\cos\varphi = 1$. The OGO sends equal power factor set–points PF_i to the WPPs.
- S4: Optimization–based operation where the system power losses are minimized under use of the WPP reactive power set–points q_i and the reference voltage u_{PCC}.

Another strategy might be the operation of the VSC–HVDC at unity power factor and a dispatch of voltage set–points to the WPPs. Nevertheless, this strategy is not further investigated in this study as it is very similar to strategy S3b. The considered reactive power strategies differ in terms of the control concept, for instance, S1, S2, S3a and S3b are conventional control strategies and S4 is the proposed optimization–based control algorithm. The VSC–HVDC regulates a constant reference voltage of $u_{\mathrm{PCC}} = 1\,\mathrm{p.u.}$ at the PCC bus for the conventional strategies, whereas for strategy S4 the reference voltage is a control variable of the optimization. The OLTCs of the WPP transformers operate independently in local control mode for all strategies. Except for the benchmark case S0, the internal Q set–points inside the WPP are dispatched equally among the WTs. In case of the optimization–based strategy S4 there are additional data exchange requirements between the controllers communicating through the existing channels: each respective WPPC has to provide the measured or estimated active power p_i to the CC and receives a reactive power SP q_i. The strategies S3a and S3b require the communication of reactive power or PF set–points from the CC to the WPPC, respectively. Table I gives an overview of the concepts and their respective communication and control principles.

2.3. Optimization problem formulation

Benchmark strategy S0 and strategy S4 use different optimization approaches to operate the system, respectively. The optimization problems are defined in the following.

DOI: 10.1002/we

Table I. Summary of the reactive power management strategies. Main differences are highlighted in **bold**. The symbols $\rightarrow$ and $\rightleftarrows$ stand for unidirectional and bidirectional communication, respectively.

Strategy	Principle	Control				
		Communication interfaces	WTs	WPPs	VSC–HVDC	OLTC of WPP transformer
S0	Benchmark (overall optimization)	CC$\rightleftarrows$WTC, CC$\rightleftarrows$VSCC	**Q SP from CC**	None	**Reference voltage SP by CC**	Inactive
S1	No Q by WTs	None	**local** ($\cos\varphi = 1$)	None	Local	Local to $1\,\mathrm{p.u.}$ at MV–side
S2	No Q by WPPs	WPPC $\rightarrow$ WTC	Q SP by WPPC	**Local** ($\cos\varphi = 1$)	Local	Local to $1\,\mathrm{p.u.}$ at MV–side
S3a	No Q by VSC, Q dispatch to WPPs	WPPC$\rightarrow$VSCC , WPPC$\rightarrow$WTC	Q SP by WPPC	**Q SP by VSCC**	Local ($\cos\varphi = 1$)	Local to $1\,\mathrm{p.u.}$ at MV–side
S3b	No Q by VSC , PF dispatch to WPPs	WPPC$\rightarrow$VSCC , WPPC$\rightarrow$WTC	Q SP by WPPC	**PF SP by VSCC**	Local ($\cos\varphi = 1$)	Local to $1\,\mathrm{p.u.}$ at MV–side
S4	Offshore grid optimization	CC$\rightleftarrows$WPPC, CC$\rightleftarrows$VSCC , WPPC$\rightarrow$WTC	Q SP by WPPC	**Q SP by CC**	**Reference voltage SP by CC**	Local to $1\,\mathrm{p.u.}$ at MV–side

DOI: 10.1002/we

2.3.1. Benchmark strategy S0

An overall optimization of the power losses in the system is defined by (4)-(12), being $\boldsymbol{x}$ the design vector and $f(\boldsymbol{x})$ the objective function to minimize.

$$\boldsymbol{x} = \left[u_{\text{PCC}}, q_1, q_2, \ldots, q_t\right]^\top \tag{4}$$

$$\text{Min. } f(\boldsymbol{x}) = \sum_{i=1}^{n} P^{\text{loss}}_{\text{WPP}_i,\text{HV}} + P^{\text{loss}}_{\text{off. grid}} + P^{\text{loss}}_{\text{VSC}} \tag{5}$$

$s.t.:$

$$0 = -p_r + \sum_{s=1}^{\boldsymbol{N}_{\text{bus}}} |u_r||u_s|(G_{rs}\cos\theta_{rs} + B_{rs}\sin\theta_{rs}) \tag{6}$$

$$0 = -q_r + \sum_{s=1}^{\boldsymbol{N}_{\text{bus}}} |u_r||u_s|(G_{rs}\sin\theta_{rs} - B_{rs}\cos\theta_{rs}) \tag{7}$$

$$\boldsymbol{u_{\text{o,min}}} \leq \boldsymbol{u_o}(\boldsymbol{x}) \leq \boldsymbol{u_{\text{o,max}}}, \qquad o \in \boldsymbol{N}_{\text{bus}} \tag{8}$$

$$|\boldsymbol{i_l}(\boldsymbol{x})| \leq \boldsymbol{i_{\text{l,max}}}, \qquad l \in \boldsymbol{N}_{\text{brs}} \tag{9}$$

$$q_{\text{VSC,min}} \leq q_{\text{VSC}}(\boldsymbol{x}) \leq q_{\text{VSC,max}} \tag{10}$$

$$u_{\text{PCC}} \in [u_{\text{PCC,min}}, u_{\text{PCC,max}}] \tag{11}$$

$$\boldsymbol{q_t} \in [\boldsymbol{q_{\text{t,min}}}, \boldsymbol{q_{\text{t,max}}}], \qquad t \in \boldsymbol{N}_{\text{WT}} \tag{12}$$

where (6) and (7) are the power flow equations for the system. G_{rs} and B_{rs} are the real and imaginary part of the respective element in the admittance bus matrix Y_{rs}. Likewise, p_r, q_s, u_r, u_s, and θ_{rs} are the injected active power, injected reactive power, voltages at the respective bus r and s as well as the voltage angle θ_{rs} between those buses (total number of buses is N), respectively. The vectors $\boldsymbol{N}_{\text{WT}}$, $\boldsymbol{N}_{\text{bus}}$, and $\boldsymbol{N}_{\text{brs}}$ accommodate all WTs of the n WPPs, buses (except the PCC bus), and branches (lines and transformers), respectively. The bus voltages $\boldsymbol{u_o}$ are limited to the minimum and maximum admissible voltages $\boldsymbol{u_{\text{o,min}}} = 0.90\,\text{p.u.}$ and $\boldsymbol{u_{\text{o,max}}} = 1.10\,\text{p.u.}$. The highest current of both branch sides $\boldsymbol{i_l}$ is limited to the branch rating $\boldsymbol{i_{\text{l,max}}}$. Reactive power limitations for the WTs and the VSC–HVDC are introduced in (10) and (12), respectively. The reference voltage u_{PCC}, controlled at the PCC bus, is limited to $u_{\text{PCC,min}} = 0.90\,\text{p.u.}$ and $u_{\text{PCC,max}} = 1.10\,\text{p.u.}$. For the benchmark strategy, the local control mode of the OLTCs of the WPP transformers is disabled as it would counteract the overall optimization. The size of the design vector is proportional to the number of WTs t in the system which results in a calculation time of several minutes.

DOI: 10.1002/we

2.3.2. Offshore grid optimization by strategy S4

The objective of this strategy is the implementation of a loss optimization by reactive power control and respect the control and ownership boundaries discussed in Section 2.1. Thus, it performs an optimization of the offshore grid and leaves the internal reactive power control inside each WPP to the WPPC itself following the same control structure as the conventional strategies. In comparison to the benchmark strategy S0 a significantly smaller optimization problem results using the q_i set–points of the WPPs and u_{PCC} as decision variables. Eqs. (13)-(21) define the optimization problem ($\boldsymbol{y}$ contains the decision variables and $g(\boldsymbol{y})$ is the objective function).

$$\boldsymbol{y} = \left[u_{\text{PCC}}, q_1, q_2, \ldots, q_n\right]^\top \tag{13}$$

$$\text{Min.} \quad g(\boldsymbol{y}) = \sum_{i=1}^{n} P^{\text{loss}}_{\text{WPP}i,\text{MV}} + \sum_{i=1}^{n} P^{\text{loss}}_{\text{WPP}i,\text{trf}} + P^{\text{loss}}_{\text{off. grid}} + P^{\text{loss}}_{\text{VSC}} \tag{14}$$

$s.t.:$

$$0 = -p_r + \sum_{s=1}^{N_{\text{bus}}} |u_r||u_s|(G_{rs}\cos\theta_{rs} + B_{rs}\sin\theta_{rs}) \tag{15}$$

$$0 = -q_r + \sum_{s=1}^{N_{\text{bus}}} |u_r||u_s|(G_{rs}\sin\theta_{rs} - B_{rs}\cos\theta_{rs}) \tag{16}$$

$$\boldsymbol{u_{o,\min}} \leq \boldsymbol{u_o}(\boldsymbol{y}) \leq \boldsymbol{u_{o,\max}}, \qquad o \in \boldsymbol{N}_{\text{bus}} \tag{17}$$

$$|\boldsymbol{i_l}(\boldsymbol{y})| \leq \boldsymbol{i_{l,\max}}, \qquad l \in \boldsymbol{N}_{\text{brs}} \tag{18}$$

$$q_{\text{VSC,min}} \leq q_{\text{VSC}}(\boldsymbol{y}) \leq q_{\text{VSC,max}} \tag{19}$$

$$u_{\text{PCC}} \in [u_{\text{PCC,min}}, u_{\text{PCC,max}}] \tag{20}$$

$$\boldsymbol{q_i} \in [\boldsymbol{q_{i,\min}}, \boldsymbol{q_{i,\max}}], \qquad s \in \boldsymbol{N}_{\text{WPP}} \tag{21}$$

The objective function $g(\boldsymbol{y})$ in (14) uses the developed WPP loss functions $P^{\text{loss}}_{\text{WPP}i,\text{MV}}$ which inherently require the WPP transformer losses $P^{\text{loss}}_{\text{WPP}i,\text{trf}}$ to be considered separately. The vector $\boldsymbol{N}_{\text{WPP}}$ contains the corresponding MV–side transformer buses of the n WPPs. The constraints defined by (15) to (21) are set analogue to (6) to (12). The reactive power values at the VSC–HVDC and the respective MV–side of the WPP transformers are considered for q_{VSC} and q_1 to q_n in (19) and (21), respectively. For this strategy, similar to the conventional strategies, the OLTC of the WPP transformers operates in local control mode. The local control mode foresees to control the MV–side busbars of the respective WPP transformers to a value of around 1 p.u.. Therefore, the voltage constraints for these busbars are set to $u_{\text{o,min}} = 0.999\,\text{p.u.}$ and $u_{\text{o,max}} = 1.001\,\text{p.u.}$. As this optimization problem makes use of the approximated loss functions of the WPPs, the

DOI: 10.1002/we

design vector and the optimization problem itself are significantly smaller than for the benchmark strategy. The calculation is performed in few seconds.

2.4. Active power variation within the cluster

The performance assessment aims to cover different operating points of the system. The key performance indicator, the AEP, is then calculated with the frequency per year for each operating point and the power flowing into the DC–side of the offshore VSC–HVDC for the corresponding operating point. In the following the decision on the different operating points for the analysis is outlined.

On the one hand, each WT has an individual active power output depending on its operating status (normal operation, de–rated operation or outage) and on the local wind speed. The local wind speed might be influenced by wake effects inside the WPP where the downstream WTs see a reduced wind speed compared to the upstream WTs [32]. The active power output of a WPP p_i is affected by the combined generation of all WTs and the power losses inside the WPP. According to the analysis performed in [26], the impact of wake effects inside a single WPP on reactive power control strategies is almost negligible for the power loss variation at WPP level. The study further concludes that the power loss variation due to reactive power control correlates with the sum of active power generation by all WTs. Therefore, the internal WPP losses functions developed in Section 2.1 depend on the equal active power output of all WTs p_{WT}.

On the other hand, the individual WPPs in the cluster might be exposed to different wind conditions due to possible wakes between the WPPs [33, 34]. Such WPP cluster wake effects have been modeled for close–to–each–other–spaced WPPs in [33, 34]. It was concluded that more operational data is needed for the development of accurate models. Any active power variation between WPPs in a cluster (outages, wakes, de–rated operation) might be expressed by a stochastic variance. The variance σ^2 of active power injection in a WPP cluster comprising n WPPs is defined in (22).

$$\sigma^2 = \sum_{i=1}^{n} (p_i - \mu)^2 \qquad (22)$$

$$\text{with } \mu = \frac{1}{n} \sum_{i=1}^{n} p_i$$

where p_i is the active power injection by $\mathrm{WPP}i$ and μ is the mean value of p_1 to p_n. A variance of $\sigma^2 = 0$ means equal per–unit active power injections by the WPPs, whereas a higher σ^2 represents more distinct values.

To the knowledge of the authors, the annual frequency on active power variations between WPPs in a cluster is not available in the literature. Therefore, the calculation of the AEP in this article is performed with the results for $\sigma^2 = 0$. Additionally, the confidence level of the AEP results is supported with simulations for $\sigma^2 \neq 0$.

DOI: 10.1002/we

2.5. Operational feasibility of the proposed strategies

Taking into consideration that this work examines exclusively stationary steady–state behavior, a brief description of a possible deployment in practice is given. Table II presents a feasibility summary of the considered reactive power control strategies. The extensive calculation time of the benchmark strategy S0 and the communication requirements between CC, WTC, and VSCC disqualifies it for real implementation. Strategy S1 uses local control, where the WTs are operated at unity PF. The conventional strategies S2 to S3b rely on communication although in case of failure a local control might take over. The needed communication links are common industrial practice. Strategy S4 represents a cascaded optimization structure which controls reference voltage and reactive power set–points of the WPP. The optimization algorithm is calculated in a few seconds and is fast enough for real implementation in e.g. one–minute–long time steps.

Table II. Summary of the feasibility of reactive power control strategies.

Strategy	Principle	Feasibility	OPF execution delay	Communications
S0	Benchmark (overall optimization)	Low	Several minutes	CC to VSCC and WTs; inside WPPs
S1	No Q by WTs	Highest	N/A	Local control
S2	No Q by WPPs	High	N/A	Inside WPPs
S3a	No Q by VSC, Q dispatch to WPPs	Moderate	N/A	CC to WPPs; inside WPPs
S3b	No Q by VSC , PF dispatch to WPPs	Moderate	N/A	CC to WPPs; inside WPPs
S4	Offshore grid optimization	Moderate	Few seconds	CC to VSCC and WPPs; inside WPPs

3. CASE STUDY

The case study defines an HVDC–connected WPP cluster consisting of three WPPs. A possible geographic distribution of the WPPs is sketched in Figure 2. The main parameters are listed in Table III. The WPPs use the same turbine model based on a FSC–WT rated to $P_{\mathrm{rWT}} = 6$ MW. The reactive power capability of the WT corresponds to $\cos\varphi = 0.9$ at full power in inductive and capacitive operation, resulting in $Q_{\mathrm{rWT}} = 2.91$ Mvar available at the low–voltage–side of the WT transformer. The WT transformer steps up the internal voltage of 0.9 kV to 33 kV with a power rating of 6.7 MVA, no–load losses of 0.08%, load losses of 0.9%, and a short–circuit voltage of $u_{k0} = 6\%$. The MV collection grid submarine cables are of two cross–sections: 240 mm^2 to connect up to four WTs and 630 mm^2 to link up to seven turbines in a radial string. A standard WPP transformer rating of 280 MVA is used, with no–load losses of 0.04%, load losses of 0.3%, and

DOI: 10.1002/we

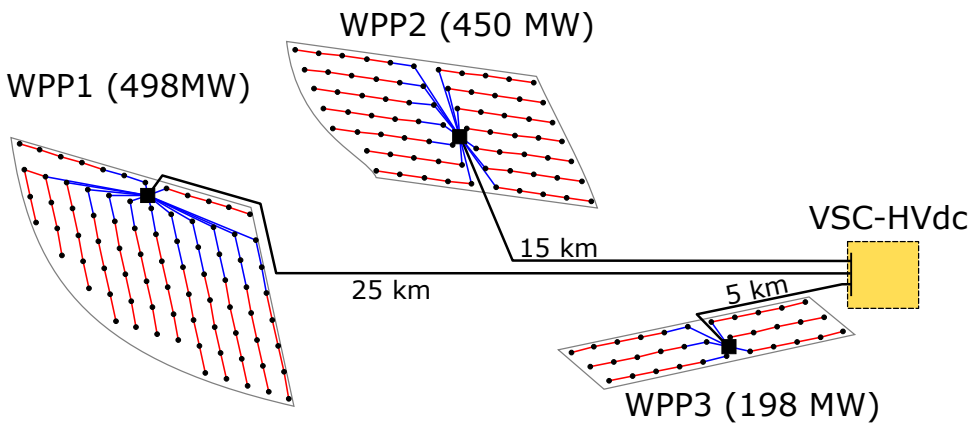

Figure 2. Possible geographical distribution of the WPP cluster under study.

a short–circuit voltage of $u_{k0} = 15\%$. The WPP transformers are equipped with OLTCs which can operate in a discrete range of $\pm 13\%$ of the turns ratio in ± 6 steps. In local control mode, the OLTCs are regulated to $u = 1\,\mathrm{p.u.}$ at the MV–side busbar within a deadband between $0.99\,\mathrm{p.u.}$ and $1.03\,\mathrm{p.u.}$ to avoid unnecessary tap changing. According to the WPP rating up to two transformers are arranged in parallel.

The WPP loss functions according to (2) are determined for the three WPPs by individual power flow calculation for a fixed voltage of $u_i = 1.0\,\mathrm{p.u.}$. The polynomial coefficients c_{jk} are calculated upon a resolution of 489 samples, by 21 equidistant values for p_{WT} and 23 values for q_i. A polynomial order of $m = 4$ results in a high accuracy measured by the coefficient of determination of $R^2 = 0.9998$ for the three WPPs. Offshore wind data for the North Sea region can be found in the Forschungsplattformen in Nord– und Ostsee (*FINO*) database [35]. The five year period wind speed data for the years 2010 to 2015 of FINO3 met mast results in a Weibull distribution with the mean wind speed $\overline{v} = 11.44$ m/s and the shape parameter $k = 2.27$ used for the AEP calculation.

4. RESULTS

This section covers first the determination of the WPP loss functions, second the results of the losses for different operating points when applying the reactive power strategies and last the AEP with the economic evaluation of the strategies.

4.1. Analysis of WPP and VSC loss functions

The WPP loss function is shown for WPP1 in Figure 3. The losses are displayed for different active power injections, namely p_{WT}, and in dependence of the reactive power set–point Q_1. It can be seen that for a small p_{WT}, there is a large gap of active power losses of approx. 5.20 MW between operation at $Q_1 = -200$ Mvar and unity power factor operation. In

DOI: 10.1002/we

Table III. Relevant parameter of the HVDC–connected WPP cluster.

WPP	WPP1	WPP2	WPP3
Nominal voltage (U_{AC}/kV)		33	
Power rating ($P_{WPP\,i}$/MW)	498	450	198
Collection grid cable length (l/km)	118	93	35
Number of turbines	83	75	33
HVAC export cable system			
Nominal voltage (U_{AC}/kV)		155	
Number of cables	3	3	1
Cross–section (A/mm^2)	630	630	800
Length (l/km)	25	15	5
Shunt compensation (Q_r/Mvar)	51.49	30.89	3.79
HVDC transmission			
Nominal voltages (U_{AC}/kV, U_{DC}/kV)		333, $\pm$320	
Converter (topology, S_r/MVA, $\cos\varphi$)		MMC, 1200 ,$\pm$0.9	
Converter loss coefficients (a / p.u., b / p.u., c / p.u.) [26]		0.0042, 0.0015, 0.0016	

contrast, for full power the difference is only around 3 MW for these operating points. Furthermore, when WPP1 is at full power production, a reactive power export results in higher losses than an import. This is due to the inductive character (consuming reactive power) of the MV collection grid at full load. It is obvious that the unity power factor operation does not inherently represent the lowest losses in the wind power plant. The polynomial coefficients for the three WPPs are listed in Table VI in the Appendix.

In contrast to the WPP loss functions, the VSC–HVDC station losses considered in this study result in flatter slopes in dependence of the q_i. The achievement of a reactive power set–point at the VSC–HVDC terminals causes less relative loss increase than at the point of connection of a WPP, mainly due to the reactive power flows provoked in the collection grid and the higher WT converter losses.

4.2. Loss reduction for $\sigma^2 = 0$

The active power losses in the system for the benchmark strategy S0 are shown in Figure 4a. It is obvious that the absolute losses increase with a higher active power injection by the WPPs. The strategies S1 to S4 are evaluated against S0 in

DOI: 10.1002/we

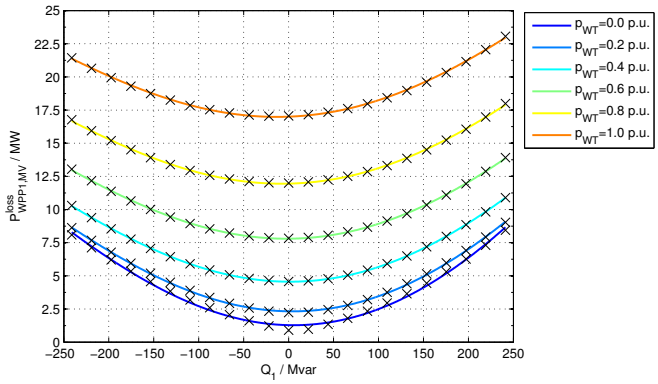

Figure 3. Loss functions of $\mathrm{WPP1}$ in dependence of reactive power set–point at the point of connection Q_1 and for different active power injections p_{WT} by the WTs (full power is of 498 MW for $\mathrm{WPP1}$). Losses are measured at the MV–side of the WPP transformer with a fixed voltage of $u = 1.0\,\mathrm{p.u.}$.

Figure 4b. The plot shows the difference between the active power losses produced for S1 to S4 and the losses for the benchmark strategy S0, respectively. It can be seen that the performance of the strategies is dependent on the sum of active power injections. The strategy S4 has the lowest loss increase varying between 0.1 and 0.8 MW. Strategy S2 performs equally to S4 in the low power range but the loss increase doubles at full power. The strategies S3a and S3b show similar results to each other. Here, it can be seen that in the low power range it is not beneficial to operate the VSC–HVDC at unity power factor (S3a and S3b), as it causes up to three times higher losses in the whole system compared to the next best strategy (S2). Strategy S1 has a good performance for the lower power range but losses increase significantly for high powers and full power.

Table IV lists selected load flow results for the full power case comprising the voltages at the grid connection point of each WPP ($u_{1\mathrm{HV}}$ to $u_{3\mathrm{HV}}$) and the PCC voltage u_{PCC} as well as reactive power injections by the WPPs at the point of connection and the VSC . It can be seen that the optimization–based strategies (S0 and S4), where u_{PCC} is not fixed to $1.0\,\mathrm{p.u.}$, the deployed overall voltage levels are around $6-7\%$ higher than for the conventional strategies. This results clearly in lower overall losses in the grid as observed earlier. Additionally, the optimization proposes reactive power injections by the WPPs which are close to the minimum power losses of the WPPs (e.g. for $\mathrm{WPP1}$ compare to Figure 3 where $\mathrm{WPP1}$ losses for $p_{\mathrm{WT}} = 1.0\,\mathrm{p.u.}$ show minimum losses at around $Q_1 = -12.8$ Mvar). For strategy S1 the high losses result from a high reactive power injection by the VSC to compensate the offshore grid. Considering the values of S3a and S3b, there is almost no difference in terms of losses but a variation of the applied reactive power SPs Q_1 to Q_3.

DOI: 10.1002/we

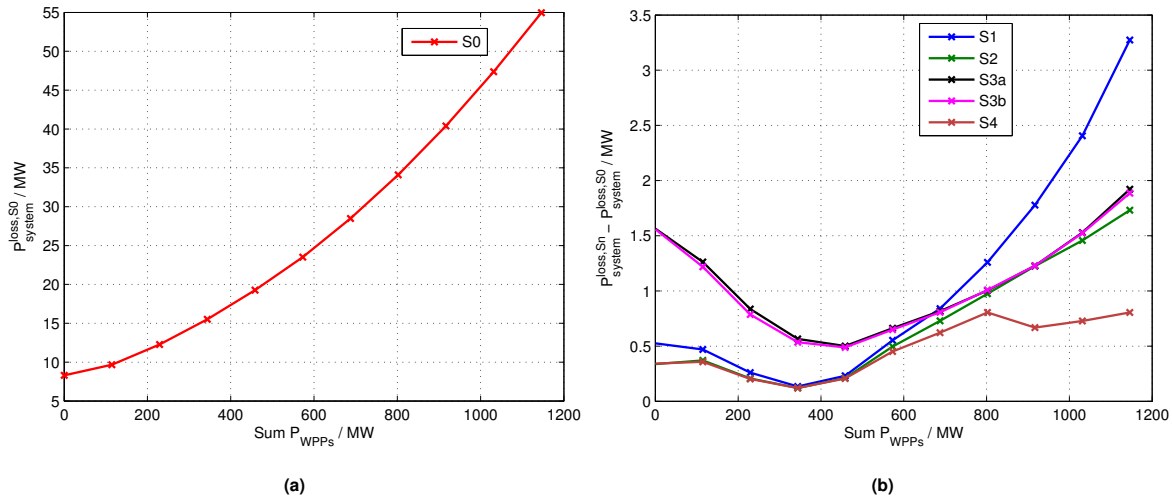

Figure 4. Absolute system losses for the benchmark case S0 in (a) and loss variation with respect to these results S0 for strategies S1 to S4 in (b). Results are shown for simulations performed under $\sigma^2 = 0$.

Table IV. Reduced load flow results for $p_1 = p_2 = p_3 = 1.0\,\mathrm{p.u.}$.

	Voltages / p.u.				Reactive power / Mvar			
	u_{PCC}	$u_{1\mathrm{HV}}$	$u_{2\mathrm{HV}}$	$u_{3\mathrm{HV}}$	Q_{VSC}	Q_1	Q_2	Q_3
S0	1.072	1.075	1.074	1.073	96.6	-28.0	-26.8	-14.5
S1	1.000	1.000	1.000	1.000	250.3	-80.7	-72.0	-31.9
S2	1.000	1.004	1.002	1.001	54.3	0.0	0.0	0.0
S3a	1.000	1.005	1.003	1.001	0.0	17.6	17.6	17.6
S3b	1.000	1.005	1.003	1.001	0.0	22.9	20.7	9.1
S4	1.066	1.069	1.068	1.066	28.7	0.0	0.0	-5.0

4.3. Loss reduction for $\sigma^2 \geq 0$

During normal operation the power output in p.u. will not be continuously equal mainly due to wind speed inequalities and WT shut–downs in the different WPPs. Consequently, a total of 1331 operating points are simulated by taking all combinations for p_1, p_2 and p_3 in 0.1 p.u. steps into account. The results are grouped by the respective variance value σ^2, calculated according to (22). Due to the extensive calculation time for the benchmark strategy S0, the loss increase is here calculated against strategy S4. Figure 5 shows the loss increase for defined variance ranges: the zero variance case $\sigma^2 = 0.0$ (11 samples), a low variance case is defined for $0.0 < \sigma^2 \leq 0.05$ (624 samples), a medium variance

DOI: 10.1002/we

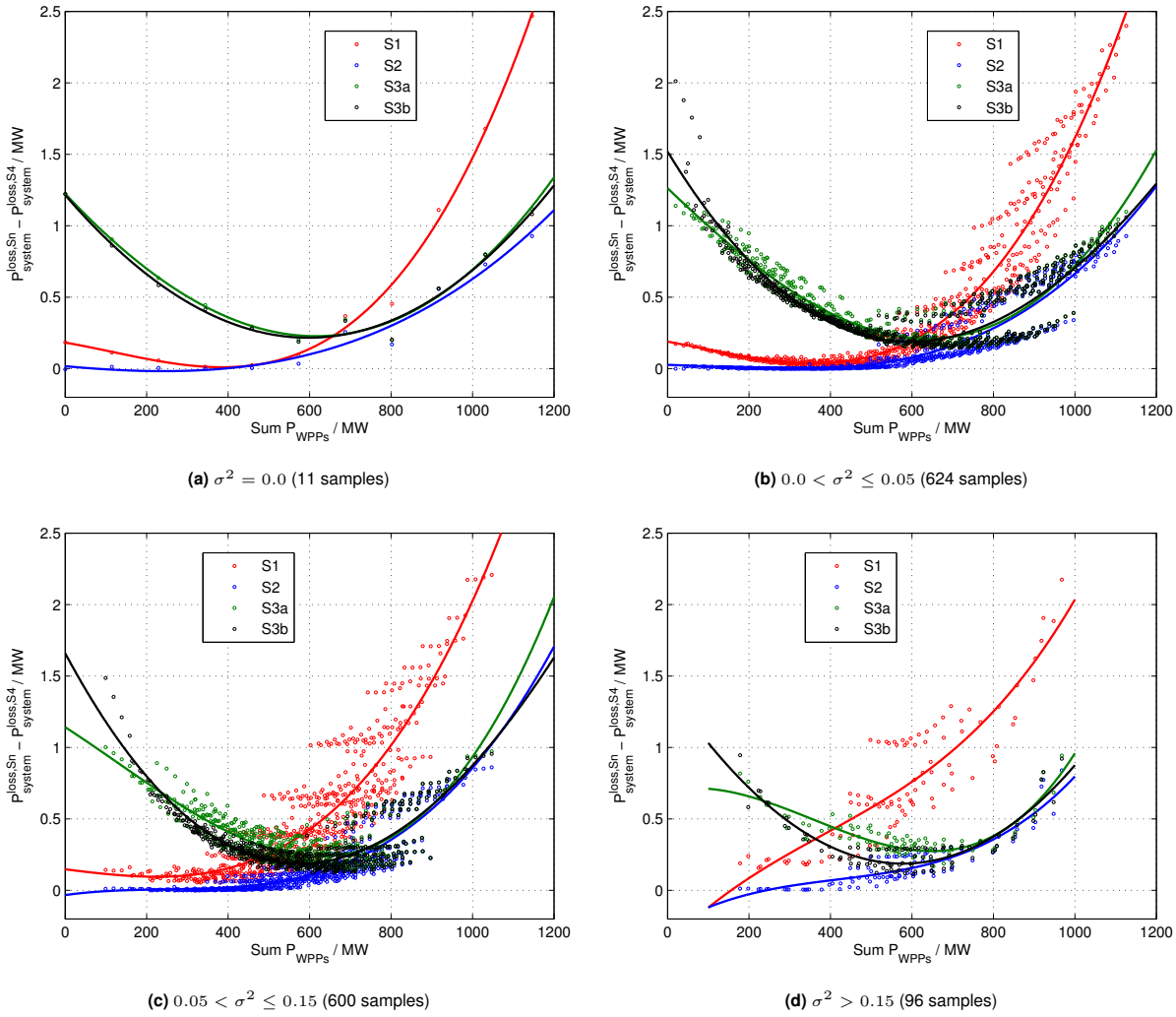

(a) $\sigma^2 = 0.0$ (11 samples)

(b) $0.0 < \sigma^2 \leq 0.05$ (624 samples)

(c) $0.05 < \sigma^2 \leq 0.15$ (600 samples)

(d) $\sigma^2 > 0.15$ (96 samples)

Figure 5. Variation of system losses with respect to S4 when gathering results of different active power injection variance groups: (a) zero, (b) low, (c) medium and (d) high variance. The solid lines are third grade polynomial approximation of these data sets.

with $0.05 < \sigma^2 \leq 0.15$ (600 samples) and a high variance for $\sigma^2 > 0.15$ (96 samples). Each data point represents one simulation and a third grade polynomial approximation of the data set is shown to ease visualization. As a first general observation, the main tendencies are kept for different values of σ^2. Especially low and medium variance, representing situations of slight wind speed differences in the cluster and/or few WT shut–downs, show similar results to $\sigma^2 = 0.0$. Nevertheless, for a high variance the performance of S1 decreases and as well as of S3a compared to S3b. The latter is caused by the advantageous power–factor–based control strategy (S3b) which avoids discrimination of unequal active power injections. The similarities observed for all σ^2 values allow the AEP calculation to be made with only equal active power injections ($\sigma^2 = 0$).

DOI: 10.1002/we

4.4. Annual energy production and economic value

The AEP of the WPP cluster, the difference in loss production against strategy S0, and the economic impact thereof are listed in Table V. As mentioned earlier, the selected simulations are based on $\sigma^2 = 0$. The economic impact depends entirely on the assumed feed–in tariff which is $100\,€\,\mathrm{MWh}^{-1}$ in this study. The most promising conventional strategy, namely S2, results in a loss increase of 8.77 GWh/y equal to 0.9 M€. The advantage against S1, S3a, and S3b is of $6.30 - 3.18$ GWh annually, in the respective order. The optimization–based strategy S4 results in the lowest loss increase of only 5.00 GWh/y compared to S0.

Table V. AEP, deviation with respect to S0 and corresponding benefit difference respective S0 due to the application of the different reactive power strategies.

Strategy	AEP GWh/y	AEP deviation to S0 GWh/y	Benefit deviation to S0 M€/y
S0	5833.2	0.00	0.0
S1	5818.1	-15.07	-1.5
S2	5824.4	-8.77	-0.9
S3a	5821.0	-12.19	-1.2
S3b	5821.3	-11.95	-1.2
S4	5828.2	-5.00	-0.5

5. CONCLUSIONS AND OUTLOOK

This paper examined five reactive power control strategies for HVDC–connected WPP clusters. A case study was defined with three WPPs connected to a VSC–HVDC. The performance of the strategies was quantified by the power losses in the system and evaluated against an optimal benchmark strategy. For the power losses a main dependence on the total active power output of the WPP cluster was found. Furthermore, the variance σ^2 of the active power injections by the respective WPPs was used to group the results. It was demonstrated that different σ^2 values did not significantly change the power losses associated to the strategies. Thus, the AEP assessment was based on equal wind speeds in the cluster. A cascaded control based on an optimization algorithm showed the best performance mainly due to a higher reference voltage imposed by the VSC–HVDC. Among the other control strategies, a continuous unity power factor operation of each WPP was favorable for the power losses. From an implementation perspective, it was depicted that the proposed

DOI: 10.1002/we

optimization–based strategy is feasible due to its low execution time and the moderate communication needs which are already industrial standard in HVDC–connected WPP clusters. However, in the current prevailing market model with split generation and transmission asset ownership in the offshore grid, the optimization–based strategy might be implemented when all owners/operators aim together to increase the AEP of the system. Furthermore, in future market implementations with a single ownership of the generation assets as well as the offshore grid comprising the HVDC link, it is clear that the proposed strategy might be very attractive for reactive power management. For the moment, the authors recommend offshore grid and WPP operators to work together and choose the appropriate reactive power control strategy for their project to gain the highest AEP.

APPENDICES

The polynomial coefficients for the WPP loss functions of WPP1 to WPP3 are shown in Table VI.

Table VI. Polynomial coefficients of WPP loss functions.

	c_{00}	c_{10}	c_{01}	c_{20}	c_{11}	c_{02}	c_{30}	c_{21}	c_{12}	c_{03}	c_{40}	c_{31}	c_{22}	c_{13}	c_{04}
WPP1	1.28	1.82	-0.36	18.17	0.37	7.79	-6.48	0.90	-3.52	0.55	2.22	-0.30	1.50	-0.37	-0.60
WPP2	1.16	1.65	-0.25	15.24	0.30	6.61	-5.75	0.80	-3.14	0.46	1.99	-0.25	1.35	-0.30	-0.55
WPP3	0.51	0.73	-0.08	6.49	0.11	2.83	-2.51	0.35	-1.38	0.19	0.87	-0.11	0.59	-0.12	-0.24

ACKNOWLEDGEMENTS

The research leading to these results has received funding from the People Programme (Marie Curie Actions) of the European Unions Seventh Framework Programme (FP7/2007-2013) under REA grant agreement number 317221, project title MEDOW. Any opinions, findings, and conclusions or recommendations expressed in this material are those of the authors and do not necessarily reflect those of General Electric.

REFERENCES

1. Xu L, Andersen BR. Grid connection of large offshore wind farms using HVDC. *Wind Energy* 2006; **9**(4):371–382, doi:10.1002/we.185.

DOI: 10.1002/we

2. Gjengedal T. Large-scale wind power farms as power plants. *Wind Energy* 2005; **8**(3):361–373, doi:10.1002/we.165.
3. CIGRE Working Group B455. HVDC connection of offshore wind power plants. *Technical Report*, CIGRE may 2015.
4. De Decker J, Kreutzkamp P. Offshore electricity grid infrastructure in Europe. *Technical Report*, OffshoreGrid 2011.
5. Wenig S, Rojas F, Schönleber K, Suriyah M, Leibfried T. Simulation framework for DC grid control and ACDC interaction studies based on modular multilevel converters. *IEEE Trans. Power Deliv.* apr 2016; **31**(2):780–788, doi:10.1109/TPWRD.2015.2417681.
6. Van Hertem D, Gomis-Bellmunt O, Liang J ((eds.)). *HVDC grids*. John Wiley and Sons, Inc.: Hoboken, NJ, USA, 2016, doi:10.1002/9781119115243.
7. Lumbreras S, Ramos A. Offshore wind farm electrical design: a review. *Wind Energy* apr 2013; **16**(3):459–473, doi:10.1002/we.1498.
8. TenneT TSO GmbH. Requirements for offshore grid connections in the grid of TenneT TSO GmbH. *Technical Report December*, TenneT TSO GmbH 2012. URL http://www.tennet.eu.
9. Curzi M, Sharma R, Martin F. In fault ride through reactive current rise time requirements of various European grid codes-analysis based on a full-converter wind turbine. *Wind Energy* jun 2016; **19**(6):1121–1133, doi:10.1002/we.1889.
10. Sáiz-Marín E, Lobato E, Egido I, Rouco L. Economic assessment of voltage and reactive power control provision by wind farms. *Wind Energy* may 2015; **18**(5):851–864, doi:10.1002/we.1734.
11. de Almeida RG, Castronuovo ED, Peças Lopes JA. Optimum generation control in wind parks when carrying out system operator requests. *IEEE Trans. Power Syst.* 2006; **21**(2):718–725, doi:10.1109/TPWRS.2005.861996.
12. Tapia A, Tapia G, Ostolaza JX. Reactive power control of wind farms for voltage control applications. *Renew. Energy* 2004; **29**(3):377–392, doi:10.1016/S0960-1481(03)00224-6.
13. Tapia G, Tapia A, Ostolaza JX. Proportional-integral regulator-based approach to wind farm reactive power management for secondary voltage control. *IEEE Trans. Energy Convers.* 2007; **22**(2):488–498, doi:10.1109/TEC.2005.858058.
14. Meegahapola LG, Vittal E, Keane A, Flynn D. Voltage security constrained reactive power optimization incorporating wind generation. *2012 IEEE Int. Conf. Power Syst. Technol. POWERCON 2012*, 2012; 1–6, doi:10.1109/PowerCon.2012.6401436.

DOI: 10.1002/we

15. Meegahapola L, Durairaj S, Flynn D, Fox B. Coordinated utilisation of wind farm reactive power capability for system loss optimisation. *Eur. Trans. Electr. Power* 2011; **21**(1):40–51, doi:10.1002/etep.410.

16. Van Pham H, Erlich I, Rueda JL. Probabilistic evaluation of voltage and reactive power control methods of wind generators in distribution networks. *IET Renew. Power Gener.* 2015; **9**(3):195–206, doi:10.1049/iet-rpg.2014.0028.

17. Nakawiro W, Erlich I, Rueda JL. A novel optimization algorithm for optimal reactive power dispatch: a comparative study. *2011 4th Int. Conf. Electr. Util. Deregul. Restruct. Power Technol.* 2011; (1):1555–1561, doi:10.1109/DRPT.2011.5994144.

18. Pappala VS, Wilch M, Singh SN, Erlich I. Reactive power management in offshore wind farms by adaptive PSO. *2007 Int. Conf. Intell. Syst. Appl. to Power Syst.*, IEEE, 2007; 1–8, doi:10.1109/ISAP.2007.4441595.

19. Wilch M, Pappala VS, Singh SN, Erlich I. Reactive power generation by DFIG based wind farms with AC grid connection. *Power Tech, 2007 IEEE Lausanne*, 2007; 626–632, doi:10.1109/PCT.2007.4538389.

20. Pham HV, Rueda JL, Erlich I. Online optimal control of reactive sources in wind power plants. *IEEE Trans. Sustain. Energy* 2014; **5**(2):608–616, doi:10.1109/TSTE.2013.2272586.

21. Martinez-Rojas M, Sumper A, Gomis-Bellmunt O, Sudrià-Andreu A. Reactive power dispatch in wind farms using particle swarm optimization technique and feasible solutions search. *Appl. Energy* 2011; **88**(12):4678–4686, doi:10.1016/j.apenergy.2011.06.010.

22. Pappala VS, Nakawiro W, Erlich I. Predictive optimal control of wind farm reactive sources. *2010 IEEE PES Transm. Distrib. Conf. Expo. Smart Solut. a Chang. World*, 2010; 1–7, doi:10.1109/TDC.2010.5484587.

23. Zhang B, Hou P, Hu W, Soltani M, Chen C, Chen Z. A reactive power dispatch strategy with loss minimization for a DFIG-based wind farm. *IEEE Trans. Sustain. Energy* jul 2016; **7**(3):914–923, doi:10.1109/TSTE.2015.2509647.

24. Erlich I, Nakawiro W, Martinez M. Optimal dispatch of reactive sources in wind farms. *2011 IEEE Power Energy Soc. Gen. Meet.*, 2011; 1–7, doi:10.1109/PES.2011.6039534.

25. Willnauer L, Marchand A. Offshore wind farm cluster design: the ClusterController. *EWEA Offshore 2013*, Frankfurt, 2013; 5.

26. Schönleber K, Ratés-Palau S, De-Prada-Gil M, Gomis-Bellmunt O. Reactive power optimization in HVDC-connected wind power plants considering wake effects. *14th Wind Integr. Work.*, Betancourt U, Ackermann T (eds.), Energynautics GmbH: Brussels, 2015.

27. Schönleber K, Collados C, Pinto RT, Ratés-Palau S, Gomis-Bellmunt O. Optimization-based reactive power control in HVDC-connected wind power plants. *Renew. Energy* aug 2017; **109**:500–509, doi:10.1016/j.renene.2017.02.081.

URL http://linkinghub.elsevier.com/retrieve/pii/S0960148117301738.

28. CIGRE Working Group B336. Special considerations for AC collector systems and substations associated with HVDC-connected wind power plants. *Technical Report*, CIGRE mar 2015.
29. Zimmerman RD, Murillo-Sanchez CE, Thomas RJ. MATPOWER: steady-state operations, planning, and analysis tools for power systems research and education. *IEEE Trans. Power Syst.* 2011; **26**(1):12–19, doi:10.1109/TPWRS.2010.2051168.
30. Daelemans G, Srivastava K, Reza M, Cole S, Belmans R. Minimization of steady-state losses in meshed networks using VSC HVDC. *2009 IEEE Power Energy Soc. Gen. Meet.*, IEEE, 2009; 1–5, doi:10.1109/PES.2009.5275450.
31. Gnanarathna UN, Gole AM, Rajapakse AD, Chaudhary SK. Loss estimation of modular multi-level converters using electro-magnetic transients simulation. *Int. Conf. Power Syst. Transients*, Delft, 2011; 2–7.
32. Hasager CB, Rasmussen L, Peña A, Jensen LE, Réthoré PE. Wind farm wake: the Horns Rev photo case. *Energies* 2013; **6**(2):696–716, doi:10.3390/en6020696.
33. Hansen KS, Barthelmie RJ, Pryor SC, Sieros G, Prospathopoulos J, Gomes VC, Schepers G, Stuart P, Young T, Rodrigo JS, *et al.*. Benchmark report on wake models at the wind farm scale. *Technical Report June 2013*, The European Energy Research Alliance Design Tools for Offshore Wind Farm Cluster 2013.
34. Hansen KS, Réthoré PE, Palma J, Hevia BG, Prospathopoulos J, Peña A, Ott S, Schepers G, Palomares A, van der Laan MP, *et al.*. Simulation of wake effects between two wind farms. *J. Phys. Conf. Ser.* jun 2015; **625**, doi:10.1088/1742-6596/625/1/012008.
35. Bundesministerium für Wirtschaft und Energie (BMWi), Projektträger Jülich (PTJ). Data of Forschungsplattform in Nord- und Ostsee (FINO). [Last accessed: August 2016] 2013. URL http://www.fino-offshore.de.